

# Influence of Atmospheric Rivers on Alaskan River Ice

Russ Limber<sup>1,2</sup>, Elias C. Massoud<sup>2</sup>, Jitendra Kumar<sup>2</sup>, Bin Guan<sup>3</sup>, Forrest M. Hoffman<sup>2</sup>

<sup>1</sup>The University of Tennessee

<sup>2</sup>Oak Ridge National Laboratory

<sup>3</sup>University of California, Los Angeles

## Key Points:

- Atmospheric Rivers (ARs) generally lead to a week-long persistent increase in daily temperature over Interior Alaska (AK)
- In AK, ARs account for 36% of total precipitation, 57% of extreme precipitation and explain 48% of interannual variability of precipitation
- AR events during the coldest months prolong the annual breakup date of river ice, while ARs closer to the breakup date have less impact.

14 **Abstract**

15 Atmospheric rivers (ARs) transport vast amounts of moisture from low to high lat-  
 16 itude regions. One region particularly impacted by ARs is Interior Alaska (AK). We  
 17 analyze the impact of ARs on the annual river ice breakup date for 25 locations in AK. We  
 18 investigate the AR-driven rise in local temperatures and explore the relationship between  
 19 ARs and precipitation, including extremes and interannual variability. We found that  
 20 the increase in local temperatures after an AR event can last for as long as one week.  
 21 Our results show that ARs account for 36% of total precipitation, explain 48% of pre-  
 22 cipitation variability, and make up 57% of extreme precipitation events. Calculating the  
 23 heat transfer between ARs and river ice, we conclude that heavy precipitation events (HPEs)  
 24 during the coldest period of the year prolong river ice breakup dates, while HPEs occur-  
 25 ring close to the breakup date have little impact on breakup timing.

26 **Plain language summary**

27 Atmospheric Rivers (ARs) are large storm systems originating in tropical regions  
 28 capable of depositing large amounts of precipitation as far north as the Arctic. Using  
 29 river ice breakup data recorded throughout Interior Alaska (AK) we set out to find whether  
 30 there exists a link between ARs and annual river ice breakup timing. We determined that  
 31 daily temperature increases can last up to one week after an AR event. We also found  
 32 that ARs account for 36% of total annual precipitation from 1980 to 2023, explain 48%  
 33 of the variability of precipitation, and make up 57% of extreme precipitation events. We  
 34 then calculated the total heat transfer between precipitation and river ice and found that  
 35 heavy precipitation events (HPEs), from both local precipitation and ARs, that occur  
 36 relatively close to river ice breakup dates, have little correlation to the breakup date. How-  
 37 ever, HPEs that occur during the coldest period of the year (typically late December to  
 38 early-February) are strongly inversely correlated with river ice breakup timing, and there-  
 39 fore prolong the breakup date.

40 **1 Introduction**

41 Atmospheric rivers (ARs) are narrow corridors of intense water vapor transport that  
 42 significantly influence hydrologic events, transporting most of the water vapor outside  
 43 of the Tropics (USDOC, 2023). It is estimated that ARs are responsible for as much as  
 44 90% of poleward water vapor transport at midlatitudes (Zhu & Newell, 1998). ARs con-  
 45 tribute to extreme precipitation events across various regions worldwide (Espinoza et al.,  
 46 2018; Massoud et al., 2019), including Western North America (Dettinger et al., 2004;  
 47 Neiman et al., 2008; Guan et al., 2010; Paul J. et al., 2011; Ralph et al., 2006; F. Mar-  
 48 tin et al., 2019; Dettinger et al., 2011) Europe (Lavers et al., 2013; Harald & Andreas,  
 49 2013), the Middle East (Massoud et al., 2020; Lashkari & Esfandiari, 2020; Esfandiari  
 50 & Shakiba, 2024), and Western South America (Viale et al., 2018). In recent years, the  
 51 impacts of ARs on the cryosphere such as Greenland (Mattingly et al., 2018) and Antarc-  
 52 tica (Gorodetskaya et al., 2014; Wille et al., 2021), have been more extensively analyzed.

53 In recent years, a growing number of works investigating the relationship between  
 54 ARs and high latitude regions has been underway. Evidence shows that between 1981  
 55 and 2020, higher atmospheric moisture content was significantly correlated with lower  
 56 sea ice coverage over almost the entire Arctic Ocean (Li et al., 2022). For those same years,  
 57 another analysis found that 100% of extreme temperature events in the Arctic (above  
 58 0 °C) coincide with the presence of ARs (Ma et al., 2023). Analyses have noted a rela-  
 59 tionship between heavy AR activity and sea ice loss, caused by increased rainfall from  
 60 moisture originating in lower latitudes (Zhang et al., 2023; MacLennan et al., 2022). How-  
 61 ever Arctic systems are complicated, as the intense moisture transport within ARs can  
 62 also result in heavy snowfall events, thus contributing to the accumulation of snowpack,

especially in mountainous regions (Saavedra et al., 2020; Guan et al., 2010). Under the right conditions, this relationship has been found to actually increase the mass balance of glaciers (Little et al., 2019). Understanding the role of ARs in the cryosphere is essential for assessing their broader impact on regional water resources and glacier dynamics in a changing climate.

While a number of works have explored the relationship between ARs and sea ice, glaciers, or ice sheets, to our knowledge there has been no analysis that investigates the relationship between ARs and Arctic river ice. Many works have used physics based processes to model the annual breakup timing and conditions of Arctic river ice (Paily et al., 1974; Ashton, 1986; T. Prowse et al., 2007; Jasek, 1998; Shen, 2010). Through such studies, it is recognized that an increase in precipitation leading to an increase in streamflow alters the hydraulics surrounding river ice breakup timing, potentially accelerating mechanical breakup events (Ashton, 1986). It has also been proposed that increased snow pack as a result of increased precipitation, contributes to breakup severity (T. D. Prowse & Beltoos, 2002). Using breakup records throughout Interior Alaska (AK) from the Alaska Pacific River Forecast Center Database (the same breakup records used in this analysis) Bieniek et al. (2011) determined that winter precipitation plays a relatively minor role in impacting the breakup timing of river ice and if anything accelerates the breakup timing as a result of increased streamflow. They go on to say that increased storm activity in the spring leads to increased surface air temperature, leading to earlier breakup dates (Bieniek et al., 2011). However, their analysis used only 4 sites (as opposed to the 25 used in this analysis) and aggregated precipitation seasonally without accounting for the interaction between winter precipitation and temperature that occurs at a finer temporal resolution. Our analysis sets out to answer the following questions: 1.) Since ARs have been known to impact Arctic systems by increasing temperatures, is there a change in air temperature in different regions of AK corresponding to the presence of ARs? 2.) How do ARs contribute to precipitation throughout AK, considering how ARs impact total annual precipitation, interannual variability, and extreme events? 3.) How do ARs impact the timing of river ice breakup, does the presence of ARs accelerate or prolong the timing of river ice breakup?

## 2 Data

### 2.1 AR Catalog

Similar to previous studies, we define ARs using integrated vapor transport (IVT) values constructed from 6-hourly values of 3-D wind and water vapor at eight pressure levels between 300 and 1,000 mb from the National Center for Environmental Protection (NCEP) reanalysis data product (Kalnay et al., 1996). AR detection is based on version3 of the tARget algorithm (Guan & Waliser, 2019; Guan, 2022). The IVT values are calculated at the original resolution from the NCEP meteorological inputs (Saha et al., 2010). Guan and Waliser (2015) developed a global AR detection algorithm, which was updated and validated later with in situ and dropsonde data (Guan, 2022). This algorithm is employed for our study, which is based on a combination of the IVT magnitude, direction, and geometry characteristics, to objectively identify ARs. Contiguous regions of enhanced IVT transport are first identified from magnitude thresholding (i.e., grid cells with IVT above the seasonally and locally dependent 85<sup>th</sup> percentile, or  $100 \frac{kg}{m*s}$ , whichever is greater) and further filtered using directional and geometry criteria requirements. Although the  $100 \frac{kg}{m*s}$  threshold is applied globally, it is intended for dry (including polar) regions since in other regions the 85th percentile is already larger than  $100 \frac{kg}{m*s}$ . The detection algorithm was applied to NCEP in its native resolution of  $2.5^\circ$ . This detection algorithm had over 90% agreement in detecting AR landfall dates when compared with other AR detection methods, for Western North America (Neiman et al., 2008), the United Kingdom (Lavers et al., 2011), and East Antarctica (Gorodetskaya et al., 2014).

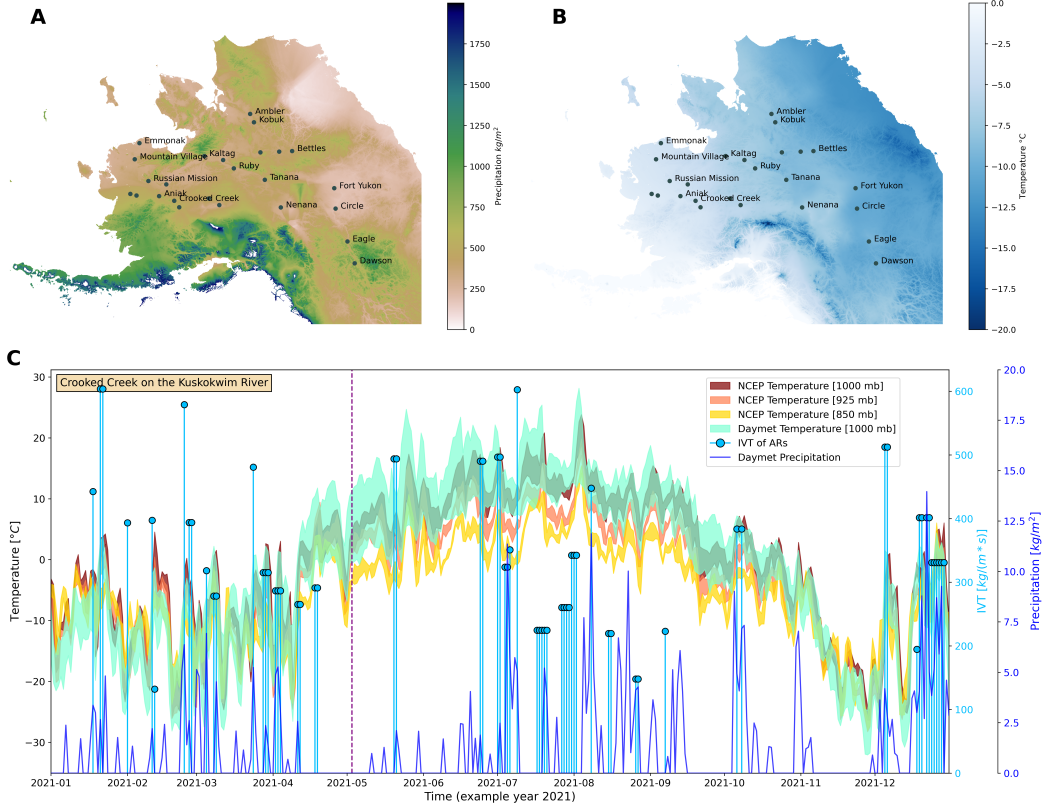


**Figure 1.** top row: (left) map showing summated precipitation for the year 2021; (right) map of average temperature for 2021. bottom row: One of the 25 locations (Crooked Creek on the Kuskokwim River) for the year 2021. Yellow, orange, red represent the temperature profiles (fill plot of  $T_{\min} - T_{\max}$ ) from NCEP temperature data at 850, 925 and 1000mb respectively. Light green represents the Daymet temperature profile. Dark blue shows modeled precipitation from Daymet while the light blue stem plots depict AR events. The vertical purple dashed line shows the breakup date for the Kuskokwim River in 2021 for Crooked Creek.

114

## 2.2 Daymet Daily Surface Weather and Climatological Summaries

115

Precipitation and daily minimum and maximum temperatures ( $T_{\min}$  and  $T_{\max}$  respectively) from Oak Ridge National Laboratory's Daymet  $1km \times 1km$  daily product were used, via the Distributed Active Archive Center (M. Thornton et al., 2022). Daymet precipitation,  $T_{\min}$  and  $T_{\max}$ , were used in our analysis as they have a strong agreement with NCEP temperature outputs for our region of interest Figure 1C. Additionally, because Daymet is derived directly from in situ instruments and meteorological stations, it represents a robust dataset for precipitation and temperature predictions across North America (P. E. Thornton et al., 2021). This dataset has been a standard for validation among several analyses related to arctic regions (Diro & Sushama, 2019; Akinsanola et al., 2024). The annual mean precipitation and temperature for the year 2021 over the AK region are shown in Figure 1AB, and Figure 1C shows the temperature profiles, precipitation and AR trends for one of those location over one year (Crooked Creek at the Kuskokwim River in 2021).

116

117

118

119

120

121

122

123

124

125

126

127

128      **2.3 River ice breakup records**

129      River ice breakup dates were obtained from the Alaska Pacific River Forecast Cen-  
 130      ter database. While exact coordinates were unavailable, locations were estimated based  
 131      on proximity to weather stations and airports, to maintain spatial consistency with in-  
 132      puts used in Daymet's meteorological models. There were 25 locations (shown in Fig-  
 133      ure 1) identified as having at least 35 breakup records between 1980 and 2023 (the cur-  
 134      rent temporal availability of Daymet), although breakup records go as far back as 1896  
 135      for some locations. The 35 breakup records threshold was used because it allowed for  
 136      the greatest number of locations with the most complete time series necessary for sta-  
 137      tistical analysis. There is always one breakup date per year, but not every year has a  
 138      recorded date, so some years are represented as empty values in the dataset. On aver-  
 139      age, recorded break up dates range from mid March to late June. This dataset has been  
 140      used in other analyses such as (Murphy et al., 2022; Brown et al., 2018; Bieniek et al.,  
 141      2011). As an example, the breakup date for Crooked Creek at the Kuskokwim River in  
 142      2021 occurred in early May and is depicted in Figure 1C with a vertical purple dashed  
 143      line.

144      **3 Methods**

145      To assess the influence of ARs on local temperature, we analyze the relationship  
 146      between the presence of an AR and the temperature change at a specific location. The  
 147      presence of an AR is represented numerically as a binary value indicating whether or not  
 148      an AR is active on a particular date. We then estimate how many days this change in  
 149      temperature lasts. To do this, we used a varying temporal window combined with a pair-  
 150      wise t-test. In other words, for each AR occurrence in the dataset, a lookback window  
 151      and forecast window each equal to  $n$  days in length was created before and after the AR  
 152      date, respectively, whereby:  $n \in \{1, 2, 3, \dots, 14\}$ . For values of  $n$  greater than one day  
 153      the mean was taken within each window for  $T_{\min}$  and  $T_{\max}$ . These aggregated temper-  
 154      atures were then calculated over all locations. Aggregated temperature pairs were as-  
 155      sessed using a one tailed pairwise t-test to check whether ARs increased the local tem-  
 156      perature over period of time  $n$  ( $\alpha = 0.05$ ).

157      We then explored how ARs contribute to precipitation, by separating AR-based  
 158      precipitation from the total amount. We then used the Wilcoxon rank-sum test (Rey &  
 159      Neuhauser, 2011) to test the hypothesis that AR events tend to produce more precip-  
 160      itation than other precipitation events. We opted to use a non-parametric test (Wilcoxon  
 161      rank-sum test) because the distributions of precipitation were shown to not be normally  
 162      distributed after log transformation using the Shapiro-Wilks test, (Shapiro & Wilk, 1965).  
 163      We also estimated the interannual variability of precipitation that ARs account for by  
 164      conducting a univariate ordinary least squares regression (OLS). For extremes, we ex-  
 165      tracted the top 5% of precipitation events and determined what fraction of those events  
 166      are associated with ARs.

167      To determine the impact that ARs have on river ice breakup timing, we used in-  
 168      formation on heat transfer estimated using Equation 1:

$$\frac{dQ}{dt} = \rho \cdot m \cdot \Delta T \quad (1)$$

169      where  $Q$  is heat flux ( $\frac{J}{m^2}$ );  $\rho$  specific heat ( $\frac{J}{g \cdot ^\circ C}$ );  $\Delta T$  is the difference of ambient tem-  
 170      perature and the river ice surface (which is estimated using  $T_{\min}$  as a proxy for ambi-  
 171      ent) ( $^\circ C$ );  $m$  the mass of the precipitation ( $kg$ ). The integral of these values over all pre-  
 172      cipitation events that occurred six months prior to the breakup date is taken with re-  
 173      spect to time. A temporal bias function (Equation 2) with tunable parameters is applied

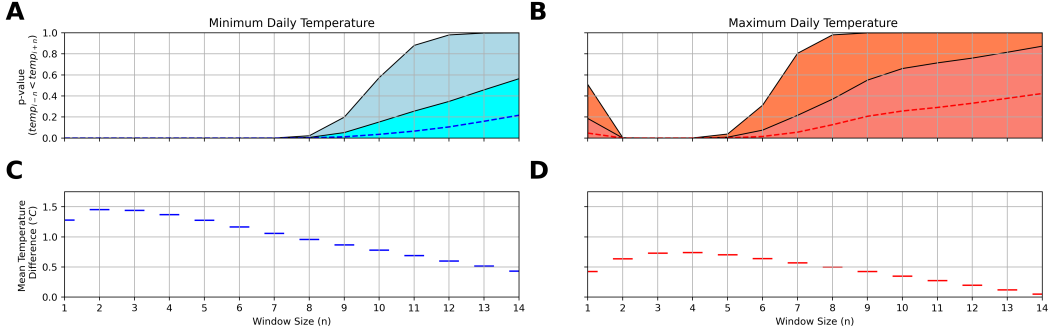


**Figure 2.** top row: the p-values of the paired t-test given the window size ( $n$ ) surrounding the AR event date (left:  $T_{\min}$ ; right:  $T_{\max}$ ). Dashed lines represent the mean p-value over the study area. For example, looking at  $T_{\min}$  on the left, the light blue represents the 25<sup>th</sup> to the 75<sup>th</sup> percentile or IQR of p-values, while the blue-grey is the 75<sup>th</sup> percentile to the maximum p-value given  $n$ . Same is true for the color transition of  $T_{\max}$ . bottom row: the average increase in temperature based on AR events, calculated from the lookback window to the forecast window.

to the heat transfer equation to assess the days of the year in which precipitation events were more impactful on breakup timing:

$$f(t; \gamma, \kappa, DOY, c) = \begin{cases} \frac{e^{-\gamma \cdot (-t - DOY)} - 1}{e^{-\gamma \cdot (t - DOY)} - 1} & \text{if } t < c \\ \frac{\kappa}{\kappa} & \text{if } t \geq c \end{cases} \quad (2)$$

where  $\gamma$  is a tunable parameter impacting the width of the exponential function;  $t$  is time in days;  $DOY$  is the day of year that the breakup date occurred;  $c$  is a tunable parameter dictating the center placement of the function;  $\kappa$  is a normalizing constant. Finally, Equation 3 is tuned over the entire hyperparameter search space for each location, optimized by selecting the parameter values that produce the Pearson correlation coefficient with the greatest absolute value.

$$\int_{t_i}^{t_{DOY}} \left( f(t; \gamma, \kappa, DOY, c) \cdot \frac{dQ}{dt} \right) dt \quad (3)$$

## 4 Results

### 4.1 AR impact on temperature

We applied the pairwise t-test comparing lookback and forecast windows of length  $n$ . Figure 2 shows the change in p-values for each value of  $n$  (top row) as well as the mean increase in temperature from the lookback window to the forecast window (bottom row). The mean temperature increase tends to be higher for  $T_{\min}$  post AR than  $T_{\max}$ , with both plots showing a clear downward trend as the length of  $n$  increases. We found that there is a statistically significant difference in  $T_{\min}$  (based on an  $\alpha = 0.05$ ) roughly 8 days before and after an AR event. This was true for all locations in the study as represented by the fill plot (Figure 2A). This increase in temperature can be as high as 1.5 °C ( $n = 2$ ) (Figure 2C). The t-test for  $T_{\max}$  implies that the presence of an AR can increase temperatures for roughly 6 days on average (Figure 2B), with an increase as high as 0.75 °C ( $n = 3, 4$ ) (Figure 2D).

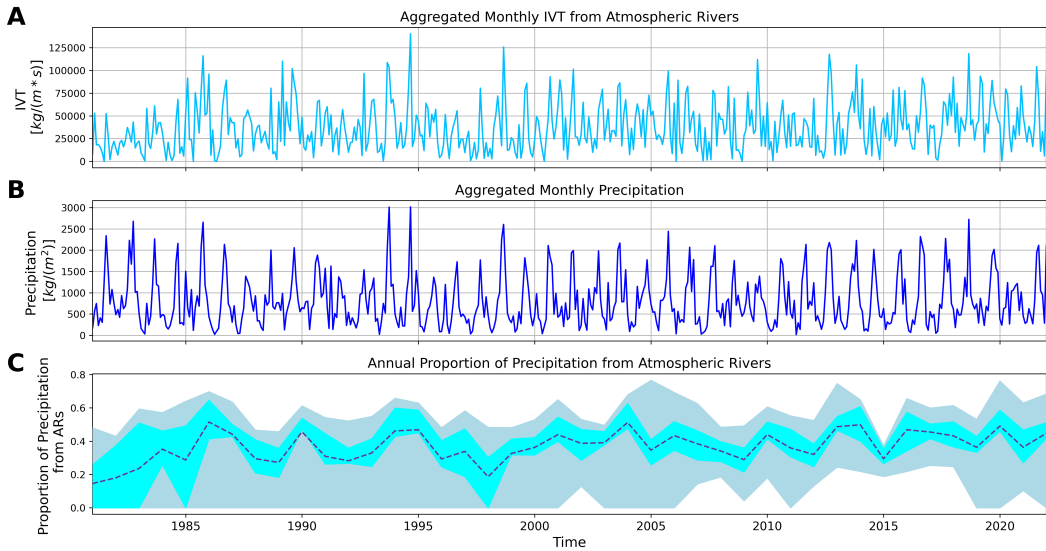


**Figure 3.** top row: time series of IVT ( $/\text{frackgm} * \text{s}$ ) aggregated monthly over all locations. middle row: time series of total precipitation ( $/\text{frackgm}^2$ ) aggregated monthly over all locations. bottom row: proportion of precipitation accounted for by ARs on an annual basis. Light blue depicts the 25<sup>th</sup> to 75<sup>th</sup> percentile (IQR) of proportion values, while the blue-grey represents proportions outside of the IQR, over all 25 locations. The dashed line represents the mean proportion.

#### 195 4.2 AR impact on precipitation

196 Figure 3 shows the AR-based IVT (Figure 3A) and total precipitation (Figure 3B)  
 197 through the span of the data record, spatially aggregated over all locations. ARs tend  
 198 to account for 36% of precipitation on average (Figure 3C), with a high degree of vari-  
 199 ability given the year and location. In 2005 and 2020, for example, ARs accounted for  
 200 nearly 80% of the total precipitation in some locations. Furthermore, the results from  
 201 the Wilcoxon rank-sum test show that precipitation from ARs tends to be greater in mag-  
 202 nitude than non-AR precipitation (test statistic =  $-83.85$ ; p-value  $\approx 0.0$ ). In addi-  
 203 tion, it was found that of the top 5% of high precipitation events (HPEs), 57% were caused  
 204 by ARs (Figure 4A). Correlating annual aggregated precipitation from ARs, to total an-  
 205 nual aggregated precipitation in a univariate OLS, we find that the coefficient of vari-  
 206 ation ( $R^2$ ) is equal to 0.48 (Figure 4B). This indicates that ARs explain about 48% of  
 207 interannual variability in precipitation, over all 25 locations.

#### 208 4.3 Transfer of energy based on Precipitation

209 To estimate the impact HPEs have on river ice breakup dates, we use Equation 3  
 210 to calculate the heat transfer between precipitation and the river ice surface. In essence,  
 211 this exercise allows us to take the energy input from precipitation (whether AR-based  
 212 or not) and determine whether or not that integrated energy accelerates or decelerates  
 213 the breakup of river ice. We find that there is a strong negative correlation between the  
 214 heat transfer and the DOY in which the river ice breaks (Figure 5A). In this context,  
 215 negative values along the y-axis of Figures 5A and 5D are interpreted as a negative heat  
 216 exchange, meaning a cooling effect on the river ice surface or a deposition of precipita-  
 217 tion below freezing. This is optimized for when the temporally-weighted bias curve is  
 218 positioned during the coldest period of the year - typically between late November and

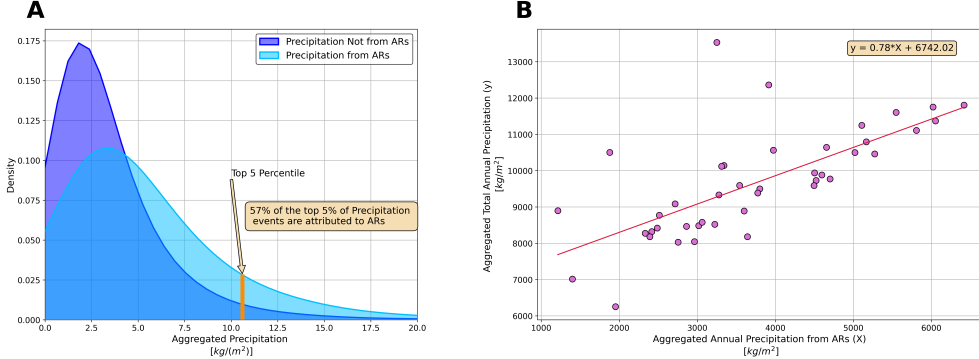


**Figure 4.** left: kernel density plots showing the distribution of local precipitation (dark blue) and precipitation from ARs (light blue). right: ordinary least squares regression plot using annual, summated precipitation from ARs, to predict total annual summated precipitation.

early February (Figure 5C). Table 1 shows the correlation for each location, after tuning parameters  $c$  and  $\gamma$  are applied to Equation 3. Table 1 also shows the center of the bias curve  $c$  (month-day) that was selected for at each location, given the integrand for precipitation used in Equation 3 (ie. Total Precipitation, Precipitation from ARs, Precipitation not from ARs). For example, Crooked Creek on the Kuskokwim River has a clear negative trend, with HPE causing a cooling effect on the river ice surface, prolonging the DOY. This relationship has a Pearson correlation coefficient ( $r_p$ ) = -0.84 and a Spearman correlation coefficient ( $r_s$ ) = -0.80, indicating that HPEs of greater magnitude, occurring during the coldest period of the year, lead to a delaying of the breakup date. The relationship between the total number of ARs that occurred six months prior to the breakup date and the DOY are shown in the center column (Figure 5B and 5E; these two plots are the same by definition) indicating that the number of AR events that occur within the six months prior to the breakup is insufficient information in correlating to breakup timing on its own. The bottom row of Figure 5 shows that the use of a bias function (Equation 2) is necessary, as simply applying the integral of Equation 1 using an equally weighted temporal bias function (the aggregated total heat transfer) is uncorrelated.

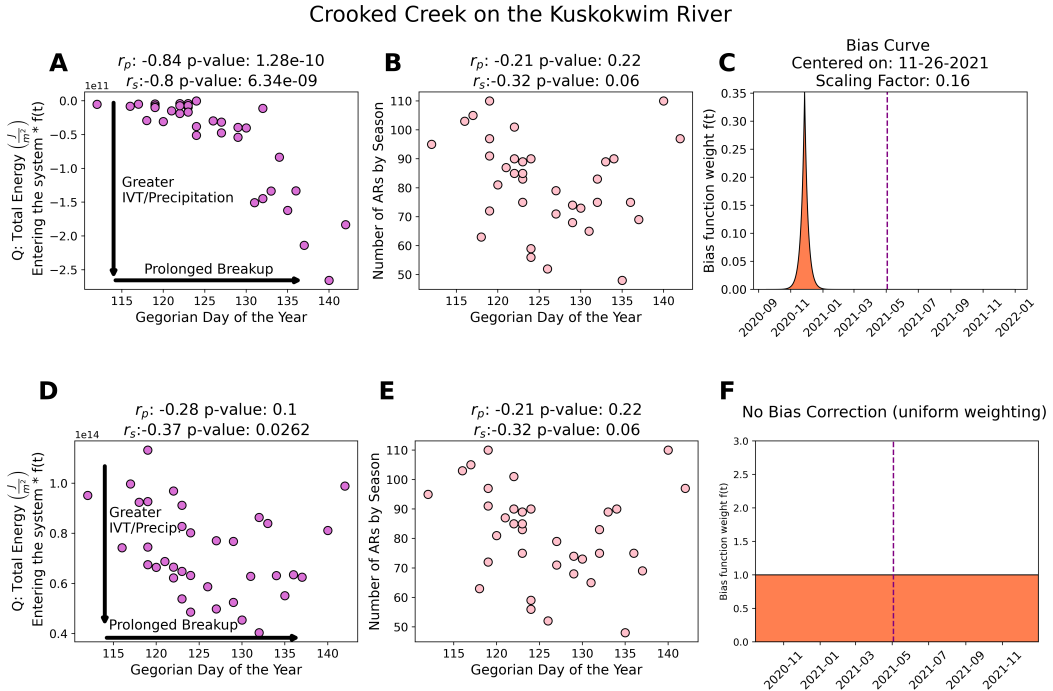


**Figure 5.** top: (left) scatter plot between thermal energy transfer and DOY; (middle) scatter plot of the number of ARs that occurred in the six months prior to the breakup date and DOY; (right) temporal bias curve for the year 2021 with the breakup date represented by the vertical dashed line. bottom: same as the top except depicting the results when a temporal bias is not utilized.

## 5 Conclusion and Discussion

This study investigated the impact atmospheric rivers (ARs) and heavy precipitation events (HPEs) have on the breakup dates of river ice in Alaska. We explored the relationship of ARs to temperature increases throughout the study domain, the contribution of ARs to various precipitation metrics, including variability and extremes, and determined the impact of ARs and HPEs on the DOY in which the ice on the surface of Alaskan rivers eventually breaks.

For temperature increases, we found that ARs generally lead to a week-long persistent increase in daily temperature over Alaska, with temperatures rising by as much as  $1.5^\circ\text{C}$  for  $T_{\min}$  and  $0.75^\circ\text{C}$  for  $T_{\max}$ . This result makes sense, as noted by many past works showing how warm moisture brought on by ARs can warm the cryosphere (Wille et al., 2021; Ma et al., 2023; Li et al., 2022; Zhang et al., 2023). For the contribution to precipitation, our results show that ARs account for a significant portion of precipitation in Alaska, contributing to 36% of total precipitation on average. They also explain 48% of interannual variability and make up 57% of extreme precipitation events (precipitation events within the top 5% of deposition). As for the relationship between ARs and river ice breakup, we show evidence that intense ARs occurring during the coldest period of the year appear to prolong the annual breakup date of river ice. Our results do not show that ARs are unique relative to local forms of precipitation in this regard (Table 1) with no evidence that increased precipitation events of any kind closer to the breakup date accelerates the breakup date. This is likely attributed to a combination of the heat transfer from precipitation, as well as changes in the river ice surface as a result of snowfall. Increased snow coverage will increase the albedo of the river surface,

259 as well as insulate it, mitigating temperature fluctuations during the coldest period of  
 260 the year.

261 Overall, understanding the role of ARs and other HPEs in the timing of river ice  
 262 break up in Alaska is crucial for predicting and managing the impacts of climate change  
 263 in the region, especially since studies have shown that AR frequency and intensity in this  
 264 region are expected to increase in a warmer world (Espinoza et al., 2018; Massoud et al.,  
 265 2019). The findings suggest that ARs contribute significantly to the hydrology and cli-  
 266 mate of Alaska, affecting temperature, precipitation, and river ice dynamics. Further re-  
 267 search in this area could help improve our understanding of ARs and their role in shap-  
 268 ing the climate of high-latitude regions.

## 269 Data Availability Statement

270 Daily Daymet precipitation and temperature data is available through the Oak Ridge  
 271 National Laboratory Distributed Active Archive at <https://daymet.ornl.gov/single-pixel/>.  
 272 The National Center for Environmental Protection temperature data can found at <https://psl.noaa.gov/data/index.html>  
 273 River ice breakup records are maintained by the Alaska Pacific River Forecast Center  
 274 at <https://www.weather.gov/aprfc/breakupMap>. The Global Atmospheric River database  
 275 is maintained by the UCLA Dataverse and can be accessed at <https://dataverse.ucla.edu/dataset.xhtml?persistentId=doi:10.1175/2010JCLI3809.1>

## 276 Acknowledgments

277 The AR database (<https://doi.org/10.25346/S6/YO15ON>) was provided by Bin Guan  
 278 via the Global Atmospheric Rivers Dataverse (<https://dataverse.ucla.edu/dataverse/ar>).  
 279 Development of the AR database was supported by NASA and the California Depart-  
 280 ment of Water Resources.

## 281 References

- 282 Akinsanola, A. A., Jung, C., Wang, J., & Kotamarthi, V. R. (2024). Evaluation  
 283 of precipitation across the contiguous united states, alaska, and puerto rico in  
 284 multi-decadal convection-permitting simulations. *Scientific Reports*, 14(1),  
 285 1238. Retrieved from <https://doi.org/10.1038/s41598-024-51714-3> doi:  
 286 10.1038/s41598-024-51714-3
- 287 Ashton, G. (1986). *River and lake ice engineering*. Water Resources Publications.  
 288 Retrieved from <https://books.google.com/books?id=xg1YVjAsnt8C>
- 289 Bieniek, P. A., Bhatt, U. S., Rundquist, L. A., Lindsey, S. D., Zhang, X., &  
 290 Thoman, R. L. (2011). Large-scale climate controls of interior alaska river  
 291 ice breakup. *Journal of Climate*, 24(1), 286 - 297. Retrieved from <https://journals.ametsoc.org/view/journals/clim/24/1/2010jcli3809.1.xml>  
 292 doi: 10.1175/2010JCLI3809.1
- 293 Brown, D. R. N., Brinkman, T. J., Verbyla, D. L., Brown, C. L., Cold, H. S., &  
 294 Hollingsworth, T. N. (2018). Changing river ice seasonality and impacts on  
 295 interior alaskan communities. *Weather, Climate, and Society*, 10(4), 625 - 640.  
 296 Retrieved from [https://journals.ametsoc.org/view/journals/wcas/10/4/wcas-d-17-0101\\_1.xml](https://journals.ametsoc.org/view/journals/wcas/10/4/wcas-d-17-0101_1.xml) doi: 10.1175/WCAS-D-17-0101.1
- 297 Dettinger, M. D., Cayan, D. R., Meyer, M. K., & Jeton, A. E. (2004). Simulated  
 298 hydrologic responses to climate variations and change in the merced, carson,  
 299 and american river basins, sierra nevada, california, 1900–2099. *Climatic  
 300 Change*, 62(1), 283–317. Retrieved from <https://doi.org/10.1023/B:CLIM.0000013683.13346.4f> doi: 10.1023/B:CLIM.0000013683.13346.4f
- 301 Dettinger, M. D., Ralph, F. M., Das, T., Neiman, P. J., & Cayan, D. R. (2011).  
 302 Atmospheric rivers, floods and the water resources of california. *Water*, 3(2),  
 303 445–478. Retrieved from <https://www.mdpi.com/2073-4441/3/2/445> doi:  
 304 10.3390/w3020445

- 307 10.3390/w3020445
- 308 Diro, G. T., & Sushama, L. (2019). Simulating canadian arctic climate at  
309 convection-permitting resolution. *Atmosphere*, 10(8). Retrieved from  
310 <https://www.mdpi.com/2073-4433/10/8/430> doi: 10.3390/atmos10080430
- 311 Esfandiari, N., & Shakiba, A. (2024). The extraordinary atmospheric rivers  
312 analysis over the middle east: Large-scale drivers, structure, effective  
313 sources, and precipitation characterization. *Dynamics of Atmospheres and*  
314 *Oceans*, 105, 101430. Retrieved from <https://www.sciencedirect.com/science/article/pii/S0377026523000817> doi: <https://doi.org/10.1016/j.dynatmoce.2023.101430>
- 315 Espinoza, V., Waliser, D. E., Guan, B., Lavers, D. A., & Ralph, F. M. (2018).  
316 Global analysis of climate change projection effects on atmospheric rivers.  
317 *Geophysical Research Letters*, 45(9), 4299-4308. Retrieved from <https://agupubs.onlinelibrary.wiley.com/doi/abs/10.1029/2017GL076968> doi:  
318 <https://doi.org/10.1029/2017GL076968>
- 319 F. Martin, R., Jonathan J., R., Jason M., C., Michael, D., Michael, A., David, R.,  
320 ... Chris, S. (2019). A scale to characterize the strength and impacts of atmo-  
321 spheric rivers. *Bulletin of the American Meteorological Society*, 100(2), 269 -  
322 289. Retrieved from <https://journals.ametsoc.org/view/journals/bams/100/2/bams-d-18-0023.1.xml> doi: 10.1175/BAMS-D-18-0023.1
- 323 Gorodetskaya, I. V., Tsukernik, M., Claes, K., Ralph, M. F., Neff, W. D., &  
324 Van Lipzig, N. P. M. (2014). The role of atmospheric rivers in anomalous snow  
325 accumulation in east antarctica. *Geophysical Research Letters*, 41(17), 6199-  
326 6206. Retrieved from <https://agupubs.onlinelibrary.wiley.com/doi/abs/10.1002/2014GL060881> doi: <https://doi.org/10.1002/2014GL060881>
- 327 Guan, B. (2022). [Data] *Global Atmospheric Rivers Database, Version 3*. UCLA  
328 Dataverse. Retrieved from <https://doi.org/10.25346/S6/Y0150N> doi: 10  
329 .25346/S6/Y0150N
- 330 Guan, B., Molotch, N. P., Waliser, D. E., Fetzer, E. J., & Neiman, P. J. (2010).  
331 Extreme snowfall events linked to atmospheric rivers and surface air tem-  
332 perature via satellite measurements. *Geophysical Research Letters*, 37(20).  
333 Retrieved from <https://agupubs.onlinelibrary.wiley.com/doi/abs/10.1029/2010GL044696> doi: <https://doi.org/10.1029/2010GL044696>
- 334 Guan, B., & Waliser, D. (2019, 12). Tracking atmospheric rivers globally: Spat-  
335 tial distributions and temporal evolution of life cycle characteristics. *Journal of*  
336 *Geophysical Research: Atmospheres*, 124. doi: 10.1029/2019JD031205
- 337 Guan, B., & Waliser, D. E. (2015). Detection of atmospheric rivers: Evaluation  
338 and application of an algorithm for global studies. *Journal of Geophysical Re-*  
339 *search: Atmospheres*, 120(24), 12514-12535. Retrieved from <https://agupubs.onlinelibrary.wiley.com/doi/abs/10.1002/2015JD024257> doi: <https://doi.org/10.1002/2015JD024257>
- 340 Harald, S., & Andreas, S. (2013). Moisture origin and meridional trans-  
341 port in atmospheric rivers and their association with multiple cyclones.  
342 *Monthly Weather Review*, 141(8), 2850 - 2868. Retrieved from <https://journals.ametsoc.org/view/journals/mwre/141/8/mwre-d-12-00256.1.xml>  
343 doi: 10.1175/MWR-D-12-00256.1
- 344 Jasek, M. (1998, July 27-31). 1998 break-up and flood on the yukon river at dawson  
345 – did el niño and climate change play a role? In H. Shen (Ed.), *Ice in surface*  
346 *waters: Proceedings of the 14th international symposium on ice* (pp. 761–768).  
347 Rotterdam: A.A. Balkema.
- 348 Kalnay, E., Kanamitsu, M., Kistler, R., Collins, W., Deaven, D., Gandin, L., ...  
349 Joseph, D. (1996). The ncep/ncar 40-year reanalysis project. *Bulletin*  
350 *of the American Meteorological Society*, 77(3), 437 - 472. Retrieved from  
351 [https://journals.ametsoc.org/view/journals/bams/77/3/1520-0477-1996\\_077\\_0437\\_tnyrp\\_2\\_0\\_co\\_2.xml](https://journals.ametsoc.org/view/journals/bams/77/3/1520-0477-1996_077_0437_tnyrp_2_0_co_2.xml) doi: 10.1175/1520-0477(1996)077(0437:

- 362 TNYRP>2.0.CO;2
- 363 Lashkari, H., & Esfandiari, N. (2020, 05). Identifying atmospheric river events and  
 364 their paths into iran. *Theoretical and Applied Climatology*, 140. doi: 10.1007/  
 365 s00704-020-03148-w
- 366 Lavers, D. A., Allan, R. P., Villarini, G., Lloyd-Hughes, B., Brayshaw, D. J., &  
 367 Wade, A. J. (2013). Future changes in atmospheric rivers and their impli-  
 368 cations for winter flooding in britain. *Environmental Research Letters*, 8(3).  
 369 Retrieved from <https://doi.org/10.1088/1748-9326/8/3/034010> doi:  
 370 10.1088/1748-9326/8/3/034010
- 371 Lavers, D. A., Allan, R. P., Wood, E. F., Villarini, G., Brayshaw, D. J., & Wade,  
 372 A. J. (2011). Winter floods in britain are connected to atmospheric  
 373 rivers. *Geophysical Research Letters*, 38(23). Retrieved from <https://agupubs.onlinelibrary.wiley.com/doi/abs/10.1029/2011GL049783> doi:  
 374 <https://doi.org/10.1029/2011GL049783>
- 375 Li, L., Cannon, F., Mazloff, M. R., Subramanian, A. C., Wilson, A. M., & Ralph,  
 376 F. M. (2022). Impact of atmospheric rivers on arctic sea ice variations. *EGU-  
 377 sphere*, 2022, 1–21. Retrieved from <https://egusphere.copernicus.org/preprints/2022/egusphere-2022-36/> doi: 10.5194/egusphere-2022-36
- 378 Little, K., Kingston, D. G., Cullen, N. J., & Gibson, P. B. (2019). The role of at-  
 379 mospheric rivers for extreme ablation and snowfall events in the southern alps  
 380 of new zealand. *Geophysical Research Letters*, 46(5), 2761–2771. Retrieved  
 381 from <https://agupubs.onlinelibrary.wiley.com/doi/abs/10.1029/2018GL081669> doi: <https://doi.org/10.1029/2018GL081669>
- 382 Ma, W., Wang, H., Chen, G., Qian, Y., Baxter, I., Huo, Y., & Seefeldt, M. W.  
 383 (2023). Wintertime extreme warming events in the high arctic: Characteristics,  
 384 drivers, trends, and the role of atmospheric rivers. *EGUsphere*. Retrieved  
 385 from [\(Preprint\)](https://doi.org/10.5194/egusphere-2023-2018) doi: 10.5194/egusphere-2023-2018
- 386 Maclennan, M. L., Lenaerts, J. T. M., Shields, C., & Wille, J. D. (2022). Contri-  
 387 bution of atmospheric rivers to antarctic precipitation. *Geophysical Research  
 388 Letters*, 49(18). Retrieved 2024-04-16, from <https://onlinelibrary.wiley.com/doi/abs/10.1029/2022GL100585> doi: 10.1029/2022GL100585
- 389 Massoud, E., Espinoza, V., Guan, B., & Waliser, D. (2019). Global cli-  
 390 mate model ensemble approaches for future projections of atmospheric  
 391 rivers. *Earth's Future*, 7(10), 1136–1151. Retrieved from <https://agupubs.onlinelibrary.wiley.com/doi/abs/10.1029/2019EF001249> doi:  
 392 <https://doi.org/10.1029/2019EF001249>
- 393 Massoud, E., Massoud, T., Guan, B., Sengupta, A., Espinoza, V., De Luna,  
 394 M., ... Waliser, D. (2020). Atmospheric rivers and precipitation in the  
 395 middle east and north africa (mena). *Water*, 12(10). Retrieved from  
 396 <https://www.mdpi.com/2073-4441/12/10/2863> doi: 10.3390/w12102863
- 397 Mattingly, K. S., Mote, T. L., & Fettweis, X. (2018). Atmospheric river im-  
 398 pacts on greenland ice sheet surface mass balance. *Journal of Geophysi-  
 399 cal Research: Atmospheres*, 123(16), 8538–8560. Retrieved from <https://agupubs.onlinelibrary.wiley.com/doi/abs/10.1029/2018JD028714> doi:  
 400 <https://doi.org/10.1029/2018JD028714>
- 401 Murphy, J. M., Garcia, S., Piston, A., Moss, J. H., Howard, K., Fergusson, E. A.,  
 402 ... others (2022). Coastal surveys in alaska and their application to salmon  
 403 run-size and harvest forecasts. *North Pacific Anadromous Fish Commission  
 404 Technical Report*(18).
- 405 Neiman, P. J., Ralph, F. M., Wick, G. A., Kuo, Y.-H., Wee, T.-K., Ma, Z., ... Det-  
 406 tinger, M. D. (2008). Diagnosis of an intense atmospheric river impacting  
 407 the pacific northwest: Storm summary and offshore vertical structure observed  
 408 with cosmic satellite retrievals. *Monthly Weather Review*, 136(11), 4398 –  
 409 4420. Retrieved from <https://journals.ametsoc.org/view/journals/mwre/>
- 410

- 417                   136/11/2008mwr2550.1.xml doi: 10.1175/2008MWR2550.1
- 418 Paily, P., Macagno, E., & Kennedy, J. (1974, 3). Winter-regime surface heat loss  
419 from heated streams. research report. *US Office of Scientific and Technical In-*  
420 *formation.* Retrieved from <https://www.osti.gov/biblio/7179276>
- 421 Paul J., N., Lawrence J., S., F. Martin, R., Mimi, H., & Gary A., W. (2011).  
422 Flooding in western washington: The connection to atmospheric rivers.  
423 *Journal of Hydrometeorology*, 12(6), 1337 - 1358. Retrieved from [https://journals.ametsoc.org/view/journals/hydr/12/6/2011jhm1358\\_1.xml](https://journals.ametsoc.org/view/journals/hydr/12/6/2011jhm1358_1.xml) doi:  
424 10.1175/2011JHM1358.1
- 425 Prowse, T., Bonsal, B., Duguay, C., & Lacroix, M. (2007). River-ice break-up/freeze-  
426 up: a review of climatic drivers, historical trends and future predictions. *An-*  
427 *nals of Glaciology*, 46, 443–451. doi: 10.3189/172756407782871431
- 428 Prowse, T. D., & Beltaos, S. (2002). Climatic control of river-ice hydrology: a review.  
429 *Hydrological Processes*, 16(4), 805-822. Retrieved from  
430 <https://onlinelibrary.wiley.com/doi/abs/10.1002/hyp.369> doi:  
431 <https://doi.org/10.1002/hyp.369>
- 432 Ralph, F. M., Neiman, P. J., Wick, G. A., Gutman, S. I., Dettinger, M. D., Cayan,  
433 D. R., & White, A. B. (2006). Flooding on california's russian river: Role  
434 of atmospheric rivers. *Geophysical Research Letters*, 33(13). Retrieved  
435 from <https://agupubs.onlinelibrary.wiley.com/doi/abs/10.1029/2006GL026689> doi: <https://doi.org/10.1029/2006GL026689>
- 436 Rey, D., & Neuhauser, M. (2011). Wilcoxon-signed-rank test. In M. Lovric (Ed.), *In-*  
437 *ternational encyclopedia of statistical science* (pp. 1658–1659). Berlin, Heidel-  
438 berg: Springer Berlin Heidelberg. Retrieved from [https://doi.org/10.1007/978-3-642-04898-2\\_616](https://doi.org/10.1007/978-3-642-04898-2_616) doi: 10.1007/978-3-642-04898-2\_616
- 439 Saavedra, F., Cortés, G., Viale, M., Margulis, S., & McPhee, J. (2020). At-  
440 mospheric rivers contribution to the snow accumulation over the southern  
441 andes (26.5° s–37.5° s). *Frontiers in Earth Science*, 8. Retrieved from  
442 <https://www.frontiersin.org/articles/10.3389/feart.2020.00261>  
443 doi: 10.3389/feart.2020.00261
- 444 Saha, S., Moorthi, S., Pan, H.-L., Wu, X., Wang, J., Nadiga, S., ... Goldberg, M.  
445 (2010). The ncep climate forecast system reanalysis. *Bulletin of the Amer-*  
446 *ican Meteorological Society*, 91(8), 1015 - 1058. Retrieved from [https://journals.ametsoc.org/view/journals/bams/91/8/2010bams3001\\_1.xml](https://journals.ametsoc.org/view/journals/bams/91/8/2010bams3001_1.xml)  
447 doi: 10.1175/2010BAMS3001.1
- 448 Shapiro, S. S., & Wilk, M. B. (1965). An analysis of variance test for normality  
449 (complete samples). *Biometrika*, 52(3-4), 591–611.
- 450 Shen, H. T. (2010). Mathematical modeling of river ice processes. *Cold Re-*  
451 *gions Science and Technology*, 62(1), 3-13. Retrieved from <https://www.sciencedirect.com/science/article/pii/S0165232X10000339> doi:  
452 <https://doi.org/10.1016/j.coldregions.2010.02.007>
- 453 Thornton, M., Shrestha, R., Wei, Y., Thornton, P., Kao, S.-C., & Wilson, B.  
454 (2022). *Daymet: Annual climate summaries on a 1-km grid for north america,* version 4 r1. ORNL Distributed Active Archive Center. Retrieved  
455 from [https://daac.ornl.gov/cgi-bin/dsviewer.pl?ds\\_id=2130](https://daac.ornl.gov/cgi-bin/dsviewer.pl?ds_id=2130) doi:  
456 10.3334/ORNLDaac/2130
- 457 Thornton, P. E., Shrestha, R., Thornton, M., Kao, S.-C., Wei, Y., & Wilson,  
458 B. E. (2021, 7 23). Gridded daily weather data for north america with  
459 comprehensive uncertainty quantification. *Scientific Data*, 8(1), 190. Re-  
460 trieval from <https://doi.org/10.1038/s41597-021-00973-0> doi:  
461 10.1038/s41597-021-00973-0
- 462 USDOC. (2023, 3). *What are atmospheric rivers?* National Oceanic and At-  
463 *mospheric Administration. Retrieved from https://www.noaa.gov/stories/what-are-atmospheric-rivers*
- 464 Viale, M., Valenzuela, R., Garreaud, R. D., & Ralph, F. M. (2018). Impacts

- of atmospheric rivers on precipitation in southern south america. *Journal of Hydrometeorology*, 19(10), 1671 - 1687. Retrieved from [https://journals.ametsoc.org/view/journals/hydr/19/10/jhm-d-18-0006\\_1.xml](https://journals.ametsoc.org/view/journals/hydr/19/10/jhm-d-18-0006_1.xml) doi: 10.1175/JHM-D-18-0006.1
- Wille, J. D., Favier, V., Gorodetskaya, I. V., Agosta, C., Kittel, C., Beeman, J. C., ... Codron, F. (2021). Antarctic atmospheric river climatology and precipitation impacts. *Journal of Geophysical Research: Atmospheres*, 126(8), e2020JD033788. Retrieved from <https://agupubs.onlinelibrary.wiley.com/doi/abs/10.1029/2020JD033788> (e2020JD033788 2020JD033788) doi: <https://doi.org/10.1029/2020JD033788>
- Zhang, P., Chen, G., Ting, M., Ruby Leung, L., Guan, B., & Li, L. (2023, March). More frequent atmospheric rivers slow the seasonal recovery of arctic sea ice. *Nature Climate Change*, 13(3), 266–273. Retrieved from <https://doi.org/10.1038/s41558-023-01599-3> doi: 10.1038/s41558-023-01599-3
- Zhu, Y., & Newell, R. E. (1998). A proposed algorithm for moisture fluxes from atmospheric rivers. *Monthly Weather Review*, 126(3), 725 - 735. Retrieved from [https://journals.ametsoc.org/view/journals/mwre/126/3/1520-0493\\_1998\\_126\\_0725\\_apafmf\\_2.0.co\\_2.xml](https://journals.ametsoc.org/view/journals/mwre/126/3/1520-0493_1998_126_0725_apafmf_2.0.co_2.xml) doi: 10.1175/1520-0493(1998)126(0725:APAFMF)2.0.CO;2

## 491 Appendix A.

**Table 1.** Table showing the Pearson correlation coefficient with the optimal center placement of the temporal bias (month-day) by location [ $r_p$ /center date of bias]

Location	Total Precipitation	Precipitation from ARs	Precipitation not from ARs
Akiak Kuskokwim River	-0.78/11-12	-0.78/2-5	-0.8/1-15
Allakaket Koyukuk River	-0.81/12-10	-0.69/10-23	-0.8/12-3
Ambler Kobuk River	-0.84/2-5	-0.67/2-5	-0.83/2-12
Aniak Kuskokwim River	-0.8/11-19	-0.81/1-29	-0.77/11-12
Bethel Kuskokwim River	-0.72/12-3	-0.75/2-5	-0.73/12-10
Bettles Koyukuk River	-0.79/2-19	-0.7/10-23	-0.81/2-12
Circle Yukon River	-0.75/2-5	-0.76/1-22	-0.74/2-12
Crooked Creek Kuskokwim River	-0.84/11-26	-0.76/2-5	-0.8/11-26
Dawson Yukon River	-0.77/10-23	-0.67/1-22	-0.75/10-23
Eagle Yukon River	-0.77/10-23	-0.79/1-22	-0.76/1-29
Emmonak Yukon River	-0.76/2-5	-0.76/1-29	-0.71/4-16
Fort Yukon Yukon River	-0.72/10-23	-0.59/2-5	-0.72/10-23
Galena Yukon River	-0.79/11-19	-0.75/1-15	-0.8/4-16
Holy Cross Yukon River	-0.75/1-8	-0.77/1-8	-0.72/1-8
Hughes Koyukuk River	-0.81/1-1	-0.78/1-15	-0.78/4-2
Kaltag Yukon River	-0.84/12-3	-0.77/12-3	-0.86/1-15
Kobuk Kobuk River	-0.81/1-8	-0.62/4-16	-0.81/1-8
McGrath Kuskokwim River	-0.81/3-26	-0.81/2-5	-0.82/4-9
Mountain Village Yukon River	-0.72/1-29	-0.76/2-5	-0.69/2-19
Nenana Tanana River	-0.71/1-1	-0.73/2-5	-0.72/1-1
Nikolai Kuskokwim River	-0.75/2-12	-0.7/2-5	-0.74/1-15
Red Devil Kuskokwim River	-0.79/12-3	-0.8/2-5	-0.78/12-3
Ruby Yukon River	-0.83/4-9	-0.78/1-15	-0.86/4-16
Russian Mission Yukon River	-0.71/11-26	-0.72/12-10	-0.68/12-3
Tanana Yukon River	-0.76/1-22	-0.7/2-5	-0.77/11-26